Discover Applied Sciences

Research

The effect of nano-natural biomaterial on stimulation of RADMSCs toward osteogenesis: an in vitro study

Farideh Alahgahi[1] · Esmail Fattahi[1] · Mohsen Saeidi[2] · Mir Mahmoud Mortazavi Roudmiane[3,4]

Received: 17 July 2023 / Accepted: 22 January 2024
Published online: 07 February 2024

Abstract
In recent years, natural biomaterials have been the focal point of most biomedical investigations. To prepare the Ostrich Eggshell/Hydroxyapatite (OE/HA) powder scaffolds, OE powder was immersed in 1% Triton X-100 for 24 h and then autoclaved twice. Medical grade HA was combined with pulverized OE at different ratios to yield three different OE/HA powder scaffolds. The resultant scaffolds underwent characterization experiments using different techniques, including FTIR, XRD, radiography, and SEM analyses. Rabbit adipose-derived mesenchymal stem cells (RADMSCs) were isolated from adipose tissues and characterized by flow cytometry. A direct contact test was performed for the cytotoxicity test using L929 cells. Cell adhesion was validated using SEM imaging, viability was assessed using DAPI and Annexin V/PI staining, and osteogenic differentiation was investigated using the ALP assay. The cytotoxicity assay using L929 cells verified that the OE/HA powder scaffold is safe and further functional experiments could be carried out. Behavioral assays, radiography, surface markers, surface topography analyses, and viability tests yielded promising results confirming cellular acceptance of the scaffold. In the present study, we provided evidence that the prepared OE/HA scaffold is not only cytocompatible but also can enhance mesenchymal stem cell adhesion, growth, and osteogenic differentiation in vitro.

Article Highlights

- Ostrich eggshell has been found to be an effective substance for stimulating mesenchymal stem cells towards bone formation.
- A new combination of a Nano-sized natural biomaterial with a resembling bone material like hydroxyapatite can enhance the growth and attachments of cells on the material surface.
- This study has proven the power of Nano calcium-based materials in altering cell lines towards the formation of bone cells.

Keywords Bone tissue engineering · Osteodifferentiation · Osteoblast · Rabbit adipose-derived mesenchymal stem cells · Ostrich eggshell powder/hydroxyapatite · Fibroblast-like cells · Osteogenic activity

✉ Esmail Fattahi, e.fattahi@iauamol.ac.ir | [1]Department of Biology, Ayatollah Amoli Branch, Islamic Azad University, Amol, Iran. [2]Stem Cell Research Center, Golestan University of Medical Sciences, Gorgan, Iran. [3]Department of Tissue Engineering, School of Paramedicine, Guilan University of Medical Sciences, Rasht, Iran. [4]Transmission Electron Microscope Lab, Biomedical Technology Wing, Sree Chitra Tirunal Institute for Medical Sciences and Technology, Trivandrum 695012, India.

1 Introduction

In the last few decades, patients have benefited from conventional therapeutic approaches in various ways. However, in the context of orthopedic surgery and bone defect reconstruction, several challenges have remained unresolved [1]. Additionally, the process of bone repair is both costly and time-consuming [2]. Damaged bones have low mechanical tolerance [2]. And significant bone trauma cannot heal spontaneously, while any type of infection can delay the healing process [3]. Reports indicate that nearly 2.2 million bone grafts are implanted annually in the US, imposing a significant burden of approximately 300 million dollars on the healthcare system [4]. The use of bone substitutes has the potential to reduce healing time and increase bone density in the damaged area [5]. Recent advances in regenerative medicine have opened up new possibilities for bone defect reconstruction. Most implants, including bone grafts from other individuals (homologous), are not readily accepted by the recipient's body and face challenges in this regard [6]. Numerous studies have reported positive results when using natural biomaterials for tissue regeneration purposes. When the right biomaterial is chosen, it can seamlessly integrate with the surrounding tissue, thereby facilitating successful tissue engineering. The high surface area of biomaterials also plays a crucial role in promoting cellular adhesion and increasing cell density. Additionally, surface roughness is an important characteristic that facilitates interactions with host tissue. It is believed that cell–matrix interactions primarily occur within a proximity of 1 nm to the surface of the biomaterial, highlighting the importance of surface properties in facilitating these interactions [7]. One widely used biomaterial that has shown beneficial effects in bone regeneration is hydroxyapatite (HA) To ensure the suitability of hydroxyapatite-polymer composites within 3D-printed grafts for medical device applications, careful optimization of both mechanical and biological properties is essential [8]. The use of 3D-printing technology presents an innovative approach to fabricating scaffolds based on hydroxyapatite (HA), offering promising opportunities for personalized bone regeneration [9]. This biomaterial possesses high osteoconductivity and resorption rates. However, it has several drawbacks, such as lacking a porous structure and ridged corners necessary for optimal cell attachment and extracellular matrix orientation.

Eggshell, as a bio-waste material, not only contains numerous minerals but also provides scaffold stability and an extraordinary topography for cell attachment. Multipotent stem cells, such as rabbit adipose-derived mesenchymal stem cells (RADMSCs), have become a focal point in bio-scaffold research due to their specific responses to distinct microenvironmental cues. In this study, the osteoinductive potential of an ostrich eggshell-hydroxyapatite (OE-HA) scaffold was assessed by seeding. The integration and osteo-induction of cells with the bio-scaffold were extensively examined by several investigators under in vitro conditions before proceeding to the final step. The main purpose of using ostrich eggshell with hydroxyapatite is to define and explore the optimal ratio of this mixture for bone healing. Despite searching through several articles, we did not find any previous studies that specifically investigated the ratio of ostrich eggshell with hydroxyapatite for better cell attachment and lacuna for cell expansion. This study aimed to fill this research gap and determine the most effective combination of these biomaterials.

2 Materials and methods

2.1 Animals

To investigate the osteoinductive capability of the OE-HA scaffold, a mixture of natural scaffold with synthetic material, rabbit adipose-derived mesenchymal stem cells (RADMSCs) were taken from dorsal part of animal, subcutaneous adipose tissue between scapula bone used in this study. Five male New Zealand White (NZW) rabbits weighing between 2.0 to 2.5 kg were obtained from the Research and Production Complex of the Pasteur Institute of Iran, located in Tehran, Iran.

The rabbits were housed under standard environmental conditions, including a temperature of 23 ± 2 °C, a humidity level of 35%, and a light/dark cycle of 12 h/12 h. The animals were provided with appropriate care and conditions, following the guidelines for the care and use of laboratory animals. The study protocol was approved by the Ethics Committee of Golestan University of Medical Sciences in Gorgan, Iran, under the reference number IR.GOUMS.REC.1397.258.

2.2 Biomaterial

A mixture of the ostrich eggshell (OE) was prepared for use in this study by cutting it into 1 cm × 1 cm slices and removing the internal membrane. The shells were then immersed in a solution of Triton X-100 (1%) for 24 h to facilitate decellularization. Afterward, they were washed with PBS and autoclaved using distilled water. This powder was passed through 0.5 mm mesh to get unique size of OE granules. To complete the decellularization process, the shells were further washed with 10% sodium hydrochloride. Subsequently, they were ground using a sterile mortar to obtain shell powder. The pulverized eggshell was then sterilized using Ethylene Oxide Sterilization (ETO) and autoclaved at 120 °C for 15 min. Hydroxyapatite (HA) powder $[Ca_{10}(OH)_2(PO_4)_6]$ (Cat No: 693863 Sigma-Aldrich Germany), which serves as the main component, was mixed with the pulverized ostrich eggshell to fabricate bone engineering scaffolds. Different ratios of OE to HA were used, including 2:1, 1:2, 1:1, 1:0, and 0:1. These designed scaffolds were utilized in various in vitro experiments as part of the study.

2.3 FTIR analysis

The structure and functional groups of the designed scaffold were analyzed using Fourier-transform infrared spectroscopy (FTIR). The FTIR analysis was conducted using a Thermo Nicolet 380 instrument, USA, which operates within the wavelength range of 500–4000 cm^{-1}. The scan speed was set at 21 scans per minute, and the resolution was 4 cm^{-1}. Spectra were recorded at room temperature during the analysis process.

2.4 XRD analysis

The designed powder scaffold underwent X-Ray Diffraction (XRD) analysis using a Philips model 17,030, Germany, diffractometer. The XRD analysis was conducted at room temperature. The instrument operated with Cu Kα radiation ($\lambda = 1.540600$ Å). The voltage was set at 30 kV, and the current was set at 40 mA. During the XRD analysis, the patterns were recorded in the 2θ range of 150 to 750, with an interval scan speed of 30/min. This allowed for the measurement of the diffraction angles and intensities, which provide information about the crystalline structure and phase composition of the scaffold material.

2.5 SEM analysis

The microstructure and surface morphology of the powder scaffold were examined using field emission scanning electron microscopy (FESEM). A Hitachi Ultra-High-Resolution Schottky, Japan, Scanning Electron Microscope model SU7000 was utilized for this purpose. The FESEM had an image resolution capability of 0.8 nm at an acceleration voltage of 15 kV. To prepare the samples for imaging, a thin layer of gold was coated onto the scaffold using a sputtering device (JEOL, JFC-1200). This gold coating helps improve the conductivity of the sample and enhances the imaging quality. Ultramicrographs of the scaffold were captured at magnifications of 50, 100, and 200 kX. These high magnification settings allowed for detailed observations of the microstructure and surface morphology, providing valuable insights into the scaffold's physical characteristics at a microscopic level.

2.6 Radiographic analysis

A radiological evaluation was conducted to assess the opacity of the designed scaffold. The analysis was performed using an X-Ray TITAN 2000 device manufactured by COMED MEDICAL in Korea. The X-ray machine was operated at 50 kV (kilovolts) and 7 mA (milliamperes) for a duration of 0.6 s. The standardized film-plane distance used during the evaluation was 14 cm. By utilizing X-ray imaging, the opacity of the scaffold could be visualized, providing information about its radiodensity and ability to block or attenuate X-rays. This evaluation helps determine the suitability of the scaffold for applications where radiopacity is desired, such as in bone defect reconstructions or other orthopedic procedures.

2.7 Cytotoxicity assay

To assess the cytotoxicity of the OE/HA scaffold, an in vitro cytotoxicity assay was performed using a direct contact test. L929 fibroblast cells at passage 3 were thawed and cultured in DMEM LG (Gibco™ Dulbecco's Modified Eagle's Medium, low

glucose, pyruvate, Cat-No: 11885084) medium. The cells were allowed to grow for 72 h until they reached confluence, with a cell density of 1×10^6 cells, in a cell culture flask. To evaluate the non-cytotoxic nature of the OE/HA scaffold, the powder scaffolds were placed in 6-well plates containing 1×10^6 cells in the cultured L929 cells. This setup allowed direct contact between the scaffold material and the cells. The purpose of this assay was to determine whether the scaffold had any adverse effects on the viability and proliferation of the L929 fibroblast cells.

2.8 RADMSCs isolation and expansion

In this study, New Zealand White (NZW) rabbits were anesthetized using intramuscular injections of ketamine (35 mg/kg) from BREMER PHARMA GMBH, Germany, and xylazine (5 mg/kg) from Sedaxylan Solution, Hyperdrug, UK. The anesthesia was administered to ensure the comfort and immobility of the rabbits during the procedure. Under aseptic conditions, adipose tissues were harvested from the rabbits. The collected adipose tissues were placed in 50 ml of PBS containing two units of penicillin to prevent contamination. The adipose tissue, weighing 15 g, was washed 4 times with sterile PBS. During each washing step, the tissue was minced into small pieces, resulting in a soup-like solution. To further process the adipose tissue, a 0.1% collagenase I solution (Sigma-Aldrich Cat-No: SCR103) was added, and the mixture was incubated at 37 °C for 60 min [12]. This step allowed for the enzymatic digestion by collagenase I on the tissue to digest the matrix and release cells and the adipose-derived mesenchymal stem cells (ADMSCs). After the collagenase reaction, the digestion was stopped by adding DMEM LG (Gibco™ Dulbecco's Modified Eagle's Medium, low glucose).

The digested tissue was then filtered through a 22 µm filter to remove any remaining tissue fragments. The resulting cell suspension was centrifuged at 2250 rpm and 4 °C for seven minutes. The pellet obtained from centrifugation contained the RADMSCs (rabbit adipose-derived mesenchymal stem cells), which were then resuspended in one ml of DMEM HG (Gibco™ Dulbecco's Modified Eagle's Medium, high glucose) and transferred into a tissue culture flask containing 4 ml of DMEM HG. The tissue culture flask was then incubated at 37 °C and 5% CO2 for 24 h. This incubation period allowed the RADMSCs to attach and proliferate within the flask, establishing a cell culture for further experiments and investigations [25].

2.9 Flow cytometry analysis of RADMSCs

To characterize the isolated RADMSCs (rabbit adipose-derived mesenchymal stem cells), the surface expression of specific markers, including CD34, CD45, CD90, and CD105, was analyzed using flow cytometry. In the experiment, RADMSCs at passage 4 were harvested and washed with PBS. The cells were then centrifuged and resuspended at a concentration of 1×10^6 cells in 100 µl of DMEM (Dulbecco's Modified Eagle's Medium) for marker characterization. For cell staining, CD34 and CD45 were used as negative markers, while CD90 and CD105 were used as positive markers for RADMSCs. Antibodies specific to these markers were used, such as CD34 (Cat. No: 14486–1-AP) and CD45 (Cat. No: 20103–1-AP) from Proteintech LTD—North America as negative markers, and CD90 (Cat. No: 20597–1-AP) and CD105 (Cat. No: 10862–1-AP) from Proteintech LTD—North America as positive markers.

The cells were incubated for 30 min in the dark to allow for antibody binding, and then rinsed with PBS to remove any unbound antibodies. Four tubes containing the stained cells were prepared for flow cytometry analysis. The flow cytometry analysis was performed using the BD FACSAria™ III Cell Sorter from BD Biosciences. The instrument allowed for the detection and quantification of the fluorescence signals emitted by the labeled cells. The data obtained from the analysis were then analyzed using FlowJo software, which is commonly used for flow cytometry data analysis. This software enabled the interpretation and characterization of the RADMSCs based on the expression levels of the specific markers [15, 16].

2.10 2.10 Cell seeding on the three-dimensional granular scaffold

To investigate the cell morphology and adhesion within the structure of the prepared OE/HA scaffolds, the scaffolds with different ratios (as presented in Table 1) were used in combination with cultured RADMSCs in 6-well cell culture plates.

The experimental procedure involved the following steps:

Table 1 The composition of OE/HA scaffolds with different ratios

OE/HA	OE/HA	OE/HA	OE/HA	OE/HA
2–1	1–2	1–1	1–0	0–1

(1) Sterile scaffolds in the culture medium were placed into the wells of a 6-well plate and incubated for 24 h. This allowed the scaffolds to stabilize and create a suitable environment for cell seeding.
(2) Passage 3 RADMSCs at a density of 0.5×10^4 cells per well were transferred from 25 cm^2 tissue culture flasks into the 6-well plates containing the scaffolds. The cells were seeded onto the scaffolds and allowed to adhere and interact with the scaffold surface.
(3) After 24 h of incubation at 37 °C and 5% CO_2, the wells were examined under an inverted microscope. The Nikon Inverted Microscope ECLIPSE Ti-S from EINST Technology, Ltd, Singapore, was used for this purpose. The microscope allowed for visual inspection of the cell morphology and adhesion within the scaffold structure.
(4) To assess the presence of cells within the scaffold structure, two staining methods were employed: 4, 6-diamidino-2-phenylindole (DAPI) staining and Annexin V/propidium iodide (PI) double staining. DAPI staining (Sigma-Aldrich, Germany, Cat No: D9542) is a commonly used fluorescent dye that binds to DNA, allowing visualization of cell nuclei. Annexin V/PI staining (Sigma-Aldrich, Germany, Cat No: 640914) is used to detect apoptotic and necrotic cells. Annexin V binds to phosphatidylserine on the cell surface, while PI stains the DNA of late-stage apoptotic or necrotic cells.

2.11 SEM analysis of OE/HA-ADMSCs

The surface microstructure and topography of the prepared OE/HA scaffolds containing cultured RADMSCs were analyzed using FESEM (Field-Emission Scanning Electron Microscopy). Prior to imaging, all samples underwent a thin layer of gold coating using a sputtering device (JEOL, JFC-1200). Cells were kept in 2.5% glutaraldehyde in 0.1 M phosphate buffer pH 7.2 -7.4 for 24–48 h. Then wash cells with 0.1 M phosphate buffer 4 times for 15 min and rinse tissue with distilled water 3 times for 5 min and finally dehydrate cells with series of dilution of ethanol from 50 to 100% for each step 20 min. Finally, it gets ready for critical point drying. The imaging process was performed using a Hitachi Ultra-High-Resolution Schottky Scanning Electron Microscope (model SU7000) operating at an accelerating voltage of 15 kV. Images were captured at magnifications of 500X, 1000X, and 5000X, with an image resolution of 0.8 nm. This imaging technique enabled the examination of the scaffold's surface characteristics, including microstructure and topography. The gold coating enhanced the conductivity of the samples, while the FESEM provided high-resolution images, allowing for detailed analysis of the scaffold and the interaction between RADMSCs and the scaffold material.

2.12 Live-dead assay

The scaffolds were immersed into the wells of 6-well plates, pre-filled with 2 ml of DMEM LG medium, and incubated for 24 h. Thereafter, passage 4 ADMSCs (Adipose-derived Mesenchymal Stem Cells) were seeded at a density of 1×10^6 cells per well into the 6-well plates and incubated for another 24 h. After the 24-h incubation period, the cells were washed with PBS and then fixed with 3.7% paraformaldehyde. To permeabilize the cell membranes and allow for intracellular staining, a 0.1% Triton X-100 solution was added for 5 min. Next, the cell-containing scaffolds underwent a washing step with PBS, followed by DAPI staining in the dark for 1 h at room temperature. Subsequently, the wells were washed with PBS again before being visualized with a Nikon Inverted fluorescent microscope at a magnification of 20X. In this assay, the nuclei of live cells were stained blue using DAPI.

Additionally, to further verify the viability of the cultured cells within the scaffold structure, another staining approach was employed. Annexin V/PI double-staining (MERK Germany, Cat No: 640914) was used, where the nuclei of cells were stained red with Annexin V, while the cytoplasmic fibrils were visualized in green. These staining techniques allowed for the evaluation of cell viability and distribution within the scaffold structure, providing valuable insights into cell survival and interaction with the scaffold material.

2.13 ALP activity

To assess the mineralization level of the osteoblastic lineage of ADMSCs in the cell culture, ALP (Alkaline Phosphatase) expression was measured using a Phosphatase substrate kit (Merk, Cat No: 33333–18-4, Germany). The ALP rate was determined using p-nitrophenyl phosphate (p-NPP) as the phosphate substrate. For intracellular ALP rate measurement, cells were lysed by multiple cycles of freezing and thawing in deionized distilled water. The culture medium was collected on days 1, 5, 9, 13, 17, and 21 after culture to obtain the secreted ALP. The collected samples were stored in liquid nitrogen until analysis. To measure ALP activity, 75 µl of each sample was transferred

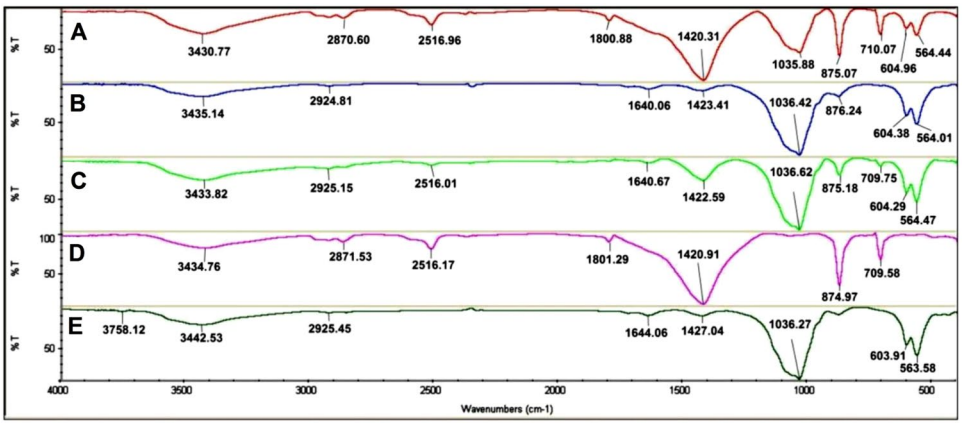

Fig. 1 TIR spectra of the three types of OE/HA scaffolds (**A**, **B**, **C**). **D** and **E** spectra represent the source materials OE and HA, respectively. Hydroxyapatite powder (**E**)

Table 2 Infrared assigned for the synthesized powder

Infrared frequency (cm^{-1})	Assignment
563/603	PO_4^{3-} bend υ_4
709/875/1427/1644/1801/2516/2871	CO_3^{2-}
1036	PO_4^{3-}bend υ_3
2925/3442	OH
603	SO_4^{2-} bend υ_4
1036	SO_4^{2-} bend υ_3

into 96-well plates for final reading. Then, 97 µl of a 5 µM p-NPP solution (New England BioLabs) was added to each well. The solution was incubated for 1 h at room temperature, and the absorbance was measured at 405 nm using an atomic absorption spectrophotometer (Shimadzu AA-6200). The ALP rate is a measure of the activity of alkaline phosphatase enzyme, which is involved in the process of osteogenesis, or bone formation. In this context, the ALP rate is being used to assess the effectiveness of mesenchymal stem cells in promoting bone formation. The ALP rate was calculated using Excel software with a standard curve and confidence level of 95% ($p < 0.05$) considered statistically significant. it was considered statistically significant, indicating that the ostrich eggshell component with hydroxyapatite can promote stem cells to osteogenesis.

3 Result

3.1 FTIR analysis

The functional groups of different scaffolds were determined using an FTIR (Fourier Transform Infrared) analyzer. Figure 1 shows the spectra labeled as D and E, which correspond to the source materials OE and HA, respectively. By analyzing the spectra labeled as A, B, and C, the presence of the source materials in the designed scaffolds can be confirmed. Table 2 provides the wavelengths and corresponding functional groups observed. The construction of OE/HA scaffolds with different ratios involved the use of OE powder (spectrum D) and medical-grade HA (spectrum E) as the source materials. In the OE spectrum (Fig. 1), the main absorption peaks at 709 cm^{-1}, 874 cm^{-1}, 1420 cm^{-1}, 1801 cm^{-1}, and 2516 cm^{-1} indicate the presence of the CO3-2 group in CaCO3 (calcite) within the OE structure. The major bands for calcite in OE appeared at 874 cm^{-1} and 1420 cm^{-1}.

Regarding the HA spectra, the peaks at 563 cm^{-1} and 603 cm^{-1} are attributed to the PO4-3 bend v4, while the peak at 1036 cm^{-1} indicates the PO4-3 bend v3. The presence of a peak at 3442 cm^{-1} is due to the stretching and bending of the hydroxyl group (O–H). The hydroxyl group is present in both OE and HA, as well as in their combination. In the HA spectrum, additional overlaying peaks at 603 cm^{-1} and 1036 cm^{-1} represent the presence of the SO4-2 group.

3.2 XRD analysis

XRD (X-ray Diffraction) analysis was conducted for three different scaffold compositions, and the obtained data were compared with those of OE and HA, which served as the source materials. The results are presented in Table 3 and Fig. 2. The extracted information from the International Centre for Diffraction Data (ICDD) was used for analysis. According to Table 3, the XRD pattern of group D corresponds to calcite (CaCO3) with the JCPDS (Joint Committee on Powder Diffraction Standards) card No. 00–047-1743. The code for Calcium Carbonate in Table 3 is 00–002-0629.

The XRD pattern of group E corresponds to hydroxyapatite and matches the ICDD reference with the JCPDS card No. 09–0432. The codes for Calcium Phosphate Hydroxide and Calcium Sulfate Hydrate in Table 3 are 01–084-1998 and 01–076-1746, respectively. The code 00–002-0629 also matches exactly with the XRD pattern. These comparisons provide evidence of the presence of specific crystalline phases, such as calcite and hydroxyapatite, in the different scaffold compositions. The XRD analysis contributes to the characterization of the scaffold structures and their similarity to the source materials.

3.3 Radiographic analysis

Radiographic analysis enables the tracking of materials, even in powder form. In this study, both pure and combined forms of materials were examined. Study groups are including A(OE/HA 2–1), B(OE/HA 1–2), C (OE/HA 1–1), D(OE/HA 1–0), E(OE/HA 0–1). Rabbit bone, ostrich eggshell (OE), and a metal coin were chosen as reference materials (Fig. 3A, E, and F, respectively). Other materials were used as test materials (Fig. 3B, C, and D, respectively). Hydroxyapatite was visible in the X-ray graph (Fig. 3B), while ostrich eggshell was visible in the radiograph (Fig. 3C). The mixture of both materials was also visible (Fig. 3D). The observed significant difference in radiopacity was attributed to the presence of the metal (Fig. 3A). The most distinguishable structures, aside from the metal coin, corresponded to the rabbit bone and OE (Fig. 3E and F, respectively).

3.4 Ultrastructure analysis by SEM

The surface morphology and topography of the prepared scaffolds were examined using SEM micrographs obtained at magnifications ranging from 50 to 200 kX. The study groups were observed at low magnification A (OE/HA 2–1), B (OE/HA 1–2), C (OE/HA 1–1), D (OE/HA 1–0), E (OE/HA 0–1), and the images can be found in Fig. 4 (A1, B1, C1, D1, and E1). The granule sizes ranged from 24 to 50 nm and exhibited irregular and ridged shapes, as shown in Fig. 4(A2, B2, C2, D2, and E2). The granules of OE had sheet-like shapes (Fig. 4D2), while the HA powder had irregular rod shapes. However, it was found that the areas covered by the sheets of OE were smaller than what is required for cell attachment.

3.5 Cytotoxicity studies

Cytotoxicity evaluations demonstrated that the scaffolds did not exhibit cytotoxic effects on L929 cells. This effect was showed the growth L929 cells beside OE/HA scaffold and showed 0% of zone around material (Fig. A and B). Throughout

Table 3 References of XRD patterns for three different types of scaffolds (A, B, and C) and the two source materials (D and E)

Test Group	Ref. Code	Score	Compound Name	Displacement [°2Th.]	Scale factor	Chemical formula	Refs.
A	98–002-1905	89	Calcite	0.220	1.097	C1 Ca1 O3	[18, 19]
	01–076-0694	44	Calcium Phosphate Hydroxide	0.200	0.276	Ca5 (P O4)3 O H	[20]
B	01–076-0694	65	Calcium Phosphate Hydroxide	0.136	1.109	Ca5 (P O4)3 O H	[20]
C	98–011-0799	92	Calcite	− 0.028	1.057	C1 Ca1 O3	[18, 19]
	00–024-0033	83	Calcium Phosphate Hydroxide	− 0.010	0.400	Ca5 (P O4)3 (O H)	[20]
D	00–002-0629	75	Calcium Carbonate	0.335	0.324	Ca C O3	[18]
E	01–084-1998	66	Calcium Phosphate Hydroxide	0.013	0.960	Ca5 (P O4)3 (O H)	[20]
	01–076-1746	48	Calcium Sulfate Hydrate	− 0.089	0.194	Ca S O4 (H2 O)2	[20]

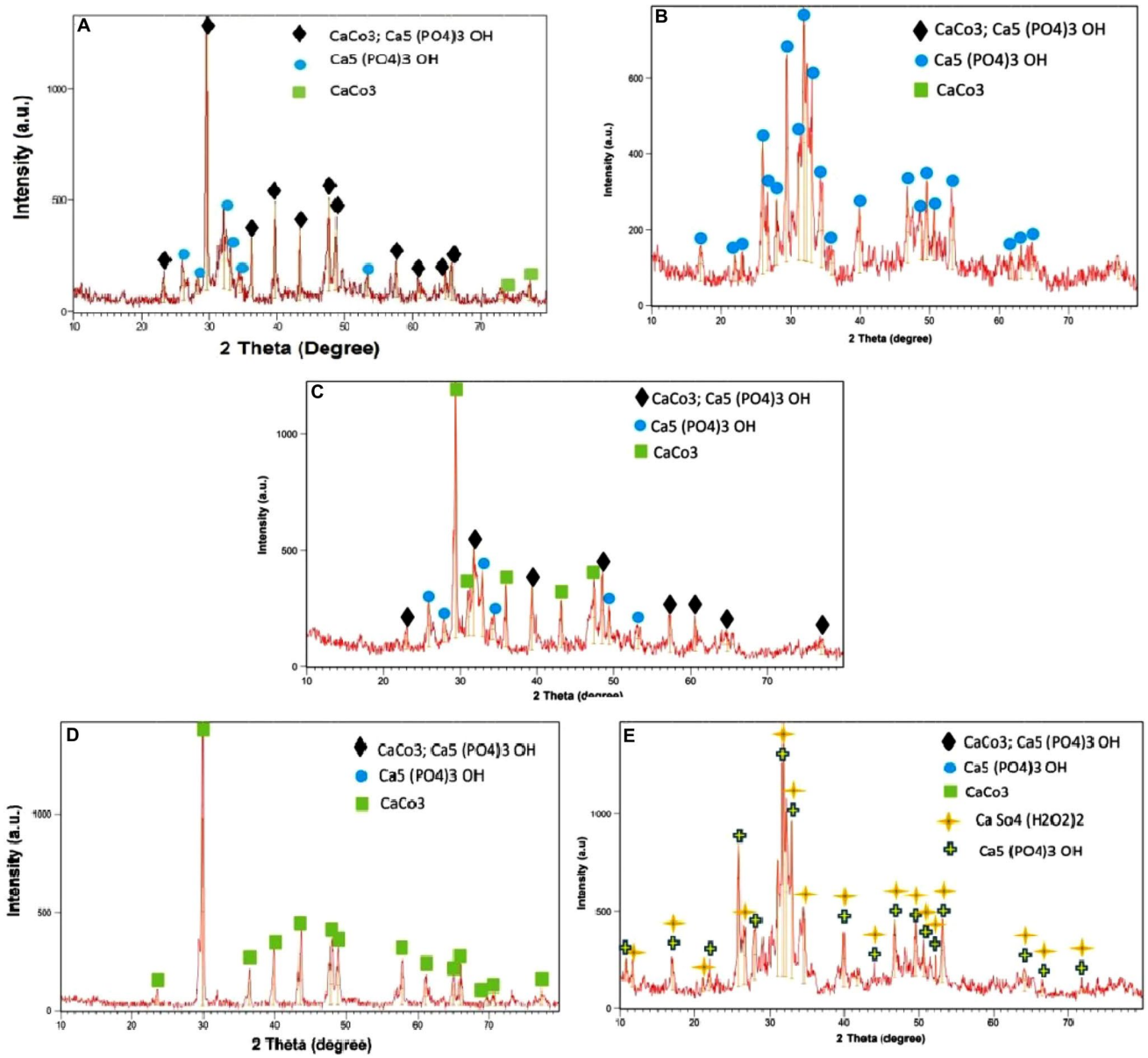

Fig. 2 XRD patterns of the three different types of OE/HA scaffold **A**, **B**, and **C** and OE **D** and HA **E** source materials

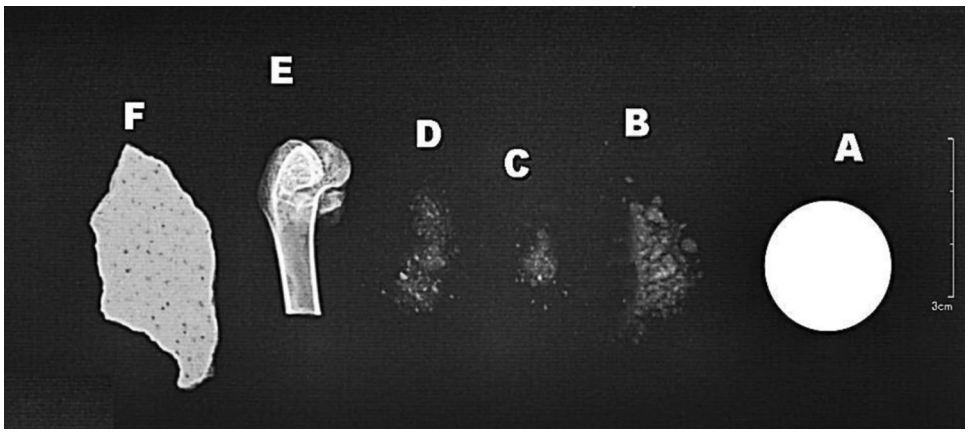

Fig. 3 The X-ray radiograph showed the radiopacity of different materials, including a metal coin, which served as a hard material sample and was visible **A**. Biomaterials for bone substitution, such as bone itself, were also visible in the radiograph, including hydroxyapatite powder **B**, OE powder **C**, and OE/HA powder **D**. Rabbit femur bone **E** and natural OE **F** were also visible in the radiograph and showed varying degrees of radiopacity

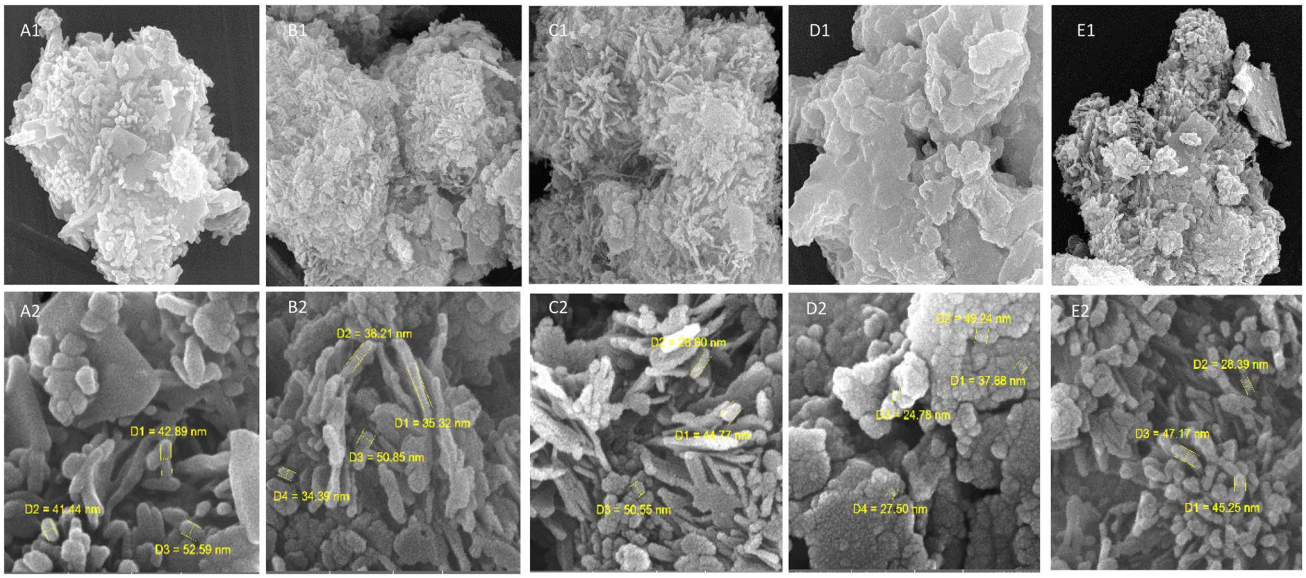

Fig. 4 SEM micrographs were taken of five different powders OE/HA scaffold to examine their surface morphology. The scaffolds had different ratios of OE/HA, including 2/1 (**A**1, **A**2), 1/2 (**B**1, **B**2), 1/1 (**C**1, **C**2), 1/0 (**D**1, **D**2), and 0/1 (**E**1, **E**2). The micrographs showed the surface morphology of the scaffolds at different magnifications, with **A**2, **B**2, **C**2, **D**2, and **E**2 showing higher magnifications compared to A1, B1, C1, D1, and E1, respectively

the experiment, 0% cell apoptosis or cell-free zones were observed in the scaffold when examining the tissue culture flasks (Fig. 5C). It is interesting to note that these phenomena occur while the cells are attached to the scaffold without any defective zones. This suggests that the scaffold is able to support cell growth and differentiation without any adverse effects on cell behavior. The absence of defective zones is particularly important, as these areas can act as weak points in the tissue engineering construct, potentially leading to failure of the regenerative process. The cells successfully adhered to the designed scaffolds, and there were no indications of vacuolated cytoplasm, indicating the high cytocompatibility of the prepared scaffold.

3.6 RADMSCs isolation and expansion under 2D and 3D cultureconditions

RADMSCs (Rabbit Adipose-Derived Mesenchymal Stem Cells) cultured and expanded in cell culture flasks were counted using a hemocytometer (Fig. 6A and B). The average total cell count per flask was determined to be approximately 3.2×10^6 cells. The adipose-derived mesenchymal stem cells were expanded as monolayers and exhibited a spindle-shaped morphology (Fig. 6B). The isolated RADMSCs were expanded under both 2D and 3D culture conditions with total cell number of 0.5×10^3 in each wells. Comparing their growth under these two conditions, it was observed that the number of RADMSCs after nine days of 3D culture was higher than that in the 2D culture conditions after the same culture period (Fig. 6). This difference can be attributed to the availability of more space in the 3D culture compared to the 2D culture conditions (Fig. 6).

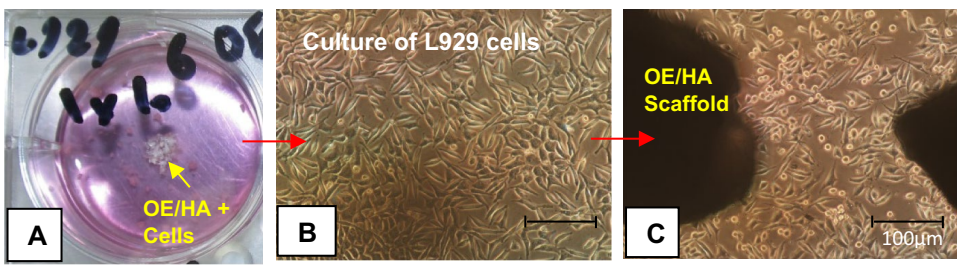

Fig. 5 Cytotoxicity assay of the OE/HA scaffold. Passage 3 L929 cells were seeded on the scaffold and incubated for 24 h. **A** shows the petri dish containing the OE/HA scaffold plus cultured L929 cells, **B** shows the cultured cells in a scaffold-free zone, and **C** is a microscopic field showing the presence of L929 cells alongside the scaffold surface

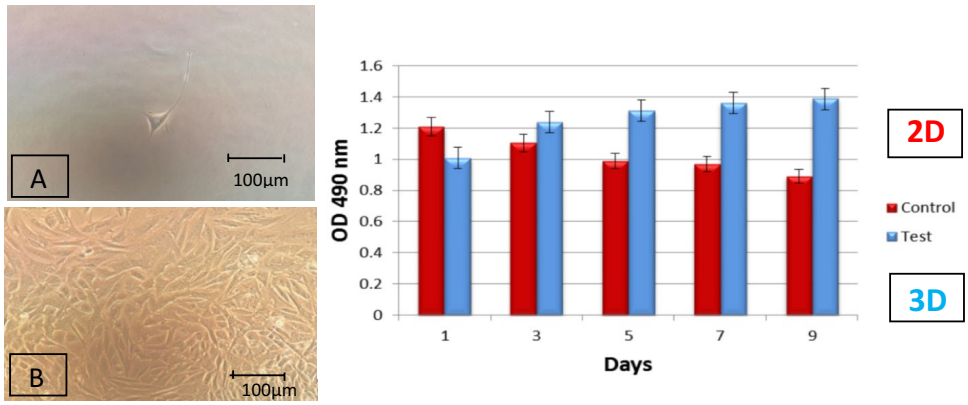

Fig. 6 RADMSCs growth under 2D and 3D culture conditions on different days

3.7 RADMSCs characterization

RADMSCs (Rabbit Adipose-Derived Mesenchymal Stem Cells) were further characterized through flow cytometric analysis of surface markers. Passage 4 RADMSCs were dissociated using trypsin and labeled with specific antibodies targeting CD34, CD45, CD90, and CD105. As depicted in Fig. 7, the isolated cells exhibited positive expression of CD90 and CD105, confirming their mesenchymal nature. Conversely, they did not show surface expression of CD34 and CD45, further supporting their mesenchymal identity. The percentage of positive cells for CD90 and CD105 markers were 99.51% and 23.25%, respectively (Fig. 7).

3.8 SEM analysis of RADMSCs presence in the structure of OE/HA scaffold

SEM images of the RADMSCs cultured on the 3D granular OE/HA scaffold clearly showed the presence of these cells within the scaffold structure. The captured images demonstrated the successful adherence of RADMSCs to the powder scaffold. The rough surface of the OE component in the scaffold structure likely played a significant role in facilitating the strong attachment and expansion of RADMSCs. This observation provides compelling evidence of the scaffold's osteoconductive effects on the cultured RADMSCs (Fig. 8).

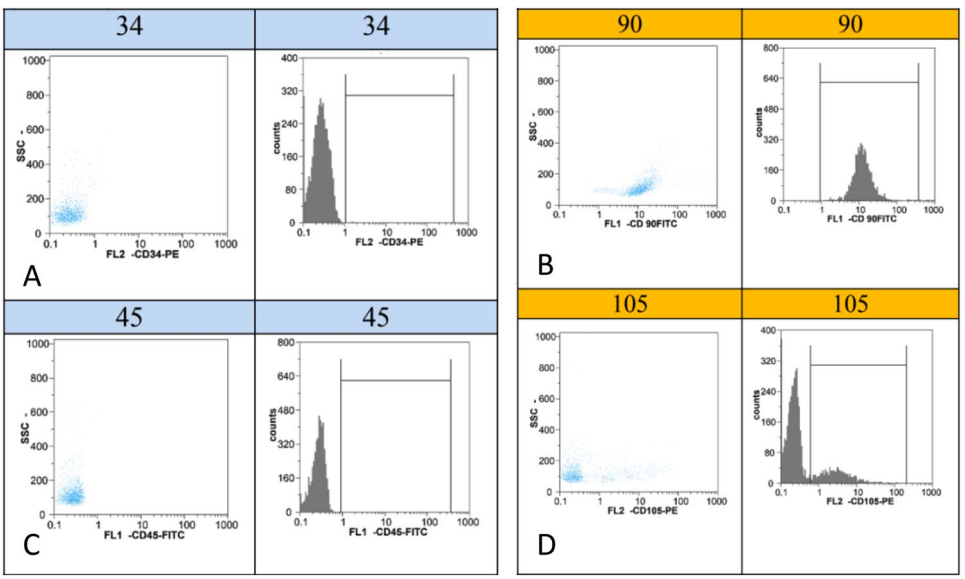

Fig. 7 Flow cytometry analysis of surface markers in the isolated RADMSCs. RADMSCs were positive for both CD90 (**B**) and CD105 (**D**) whereas they did not express CD34 (**A**) and CD45 (**C**)

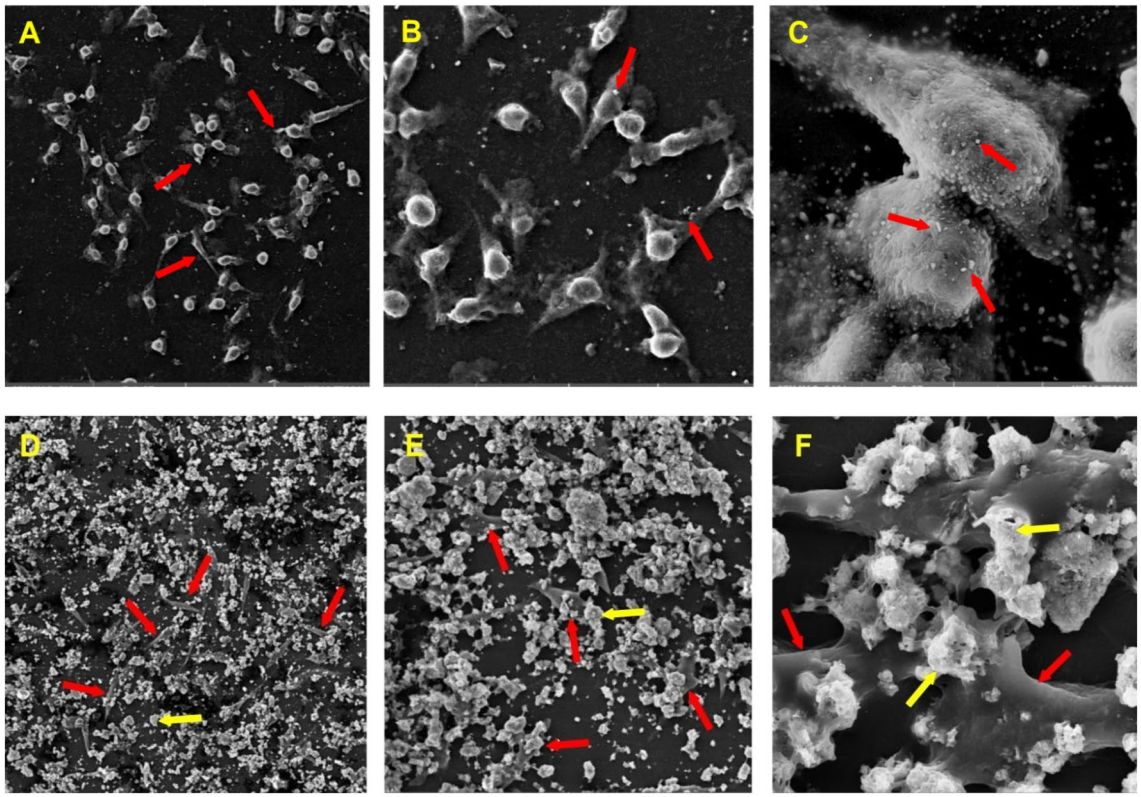

Fig. 8 SEM images of RADMSCs cultured onto the OE/HA scaffold at three different magnifications of 500 X **A** and **D**, 1000 X **B** and **E**, and 5000 X **C** and **F**. Red arrows show RADMSCs and yellow arrows show the scaffold

3.9 Live-dead assay

DAPI staining was utilized to stain the nuclei of RADMSCs (Rabbit Adipose-Derived Mesenchymal Stem Cells). The cells were washed with PBS and then permeabilized using 0.1% Triton X-100 in 20 mL of PBS for 3 min. Subsequently, they were washed again and incubated with DAPI (4′, 6-diamidino-2-phenylindole) for 5 min under dark conditions to visualize the cell nuclei.

The obtained data demonstrated the viability of RADMSCs that were seeded and cultured on the scaffolds with different compositions of OE and HA. This indicates that the prepared scaffold is cytocompatible and provides a suitable environment for RADMSC proliferation. A comparison between different combinations revealed that the powder scaffold with an OE:HA ratio of 1:2 exhibited the most favorable results (Fig. 9). To further confirm the presence of viable cells within the scaffold structure, Annexin V/PI double-staining was performed. Upon careful examination of all the wells, it was observed that all cells were alive and located adjacent to the scaffold surfaces. For the OE:HA ratio of 1:2, the cells exhibited proper orientation with visible nuclei. Even in the control well without any scaffold, the cells remained viable (Fig. 10).

3.9.1 ALP activity

ALP activity was done for 6 study groups and it is as an early-stage marker for osteogenic differentiation,was measuredby a colorimetric assay. This enzyme catalyzes p-nitrophenyl phosphate hydrolysis into p-nitrophenol and phosphate.Based on the acquired data, no significant change in ALP activity was detected on days 1 and 5. But, from day 9 to 21 ALP activity was significantly increased so that the maximal ALP activity was measured on days 17 and 21. The control group showed a lower ALP expression in comparison to the test groups. On the last day (day 21), ALP activity in the group containing the powder scaffold withan OE/HA ratio of 1:2 was the highest. Osteogenic activity was more after 13 days of culture. However, this scaffold could reveal its ability to mimic bone morphogenic protein-2 and lead

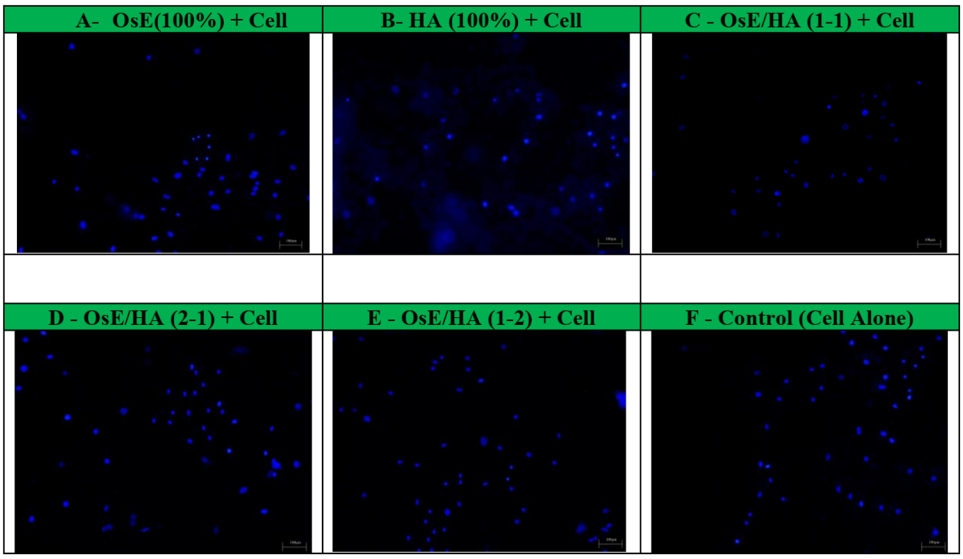

Fig. 9 Fluorescent micrographs of DAPI-stained RADMSCs in the structure of powder scaffolds with different source material compositions **A**, **B**, **C**, **D**, and **E**. In this assay, the cell nucleus is stained blue, and blue dots in the micrographs are indicative of live cells. **F** represents the control well without a scaffold

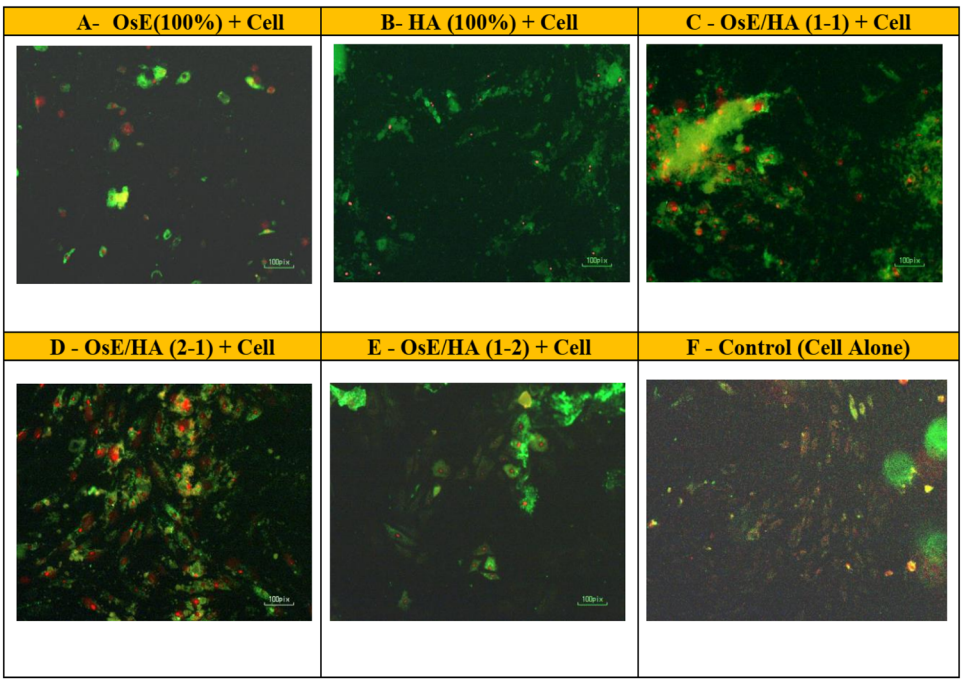

Fig. 10 Fluorescent micrographs of Annexin V/PI double staining of the cultured RADMSCs in the structure of powder scaffolds with different source materials compositions **A**, **B**, **C**, **D**, and **E**. Red colors indicate the cell nucleus and green colors indicate the cytoplasmic fibrils. **F** represents the control well without a scaffold

RADMSCs toward Osteogenic activity (Fig. 11). ALP (Alkaline Phosphatase) activity, which serves as an early-stage marker for osteogenic differentiation, was assessed using a colorimetric assay. This enzyme catalyzes the hydrolysis of p-nitrophenyl phosphate, resulting in the production of p-nitrophenol and phosphate. Based on the acquired data, there was no significant change in ALP activity observed on days 1 and 5 of the experiment. However, from day 9 to 21, there was a significant increase in ALP activity, with the highest levels measured on days 17 and 21. This indicates that osteogenic differentiation of the cells was initiated and progressed further during this time period. In comparison to the control group, the test groups exhibited higher ALP expression. On the last day of the experiment (day 21), the group that contained the powder scaffold with an OE/HA ratio of 1:2 demonstrated the highest ALP activity. The increase in ALP activity after 13 days of culture indicates that osteogenic activity was enhanced over time.

This suggests that the scaffold, with its specific composition, was able to mimic the effects of bone morphogenic protein-2 (BMP-2), a protein known to play a crucial role in bone formation, and could effectively guide RADMSCs towards osteogenic differentiation. Therefore, the results indicate that the powder scaffold with an OE/HA ratio of

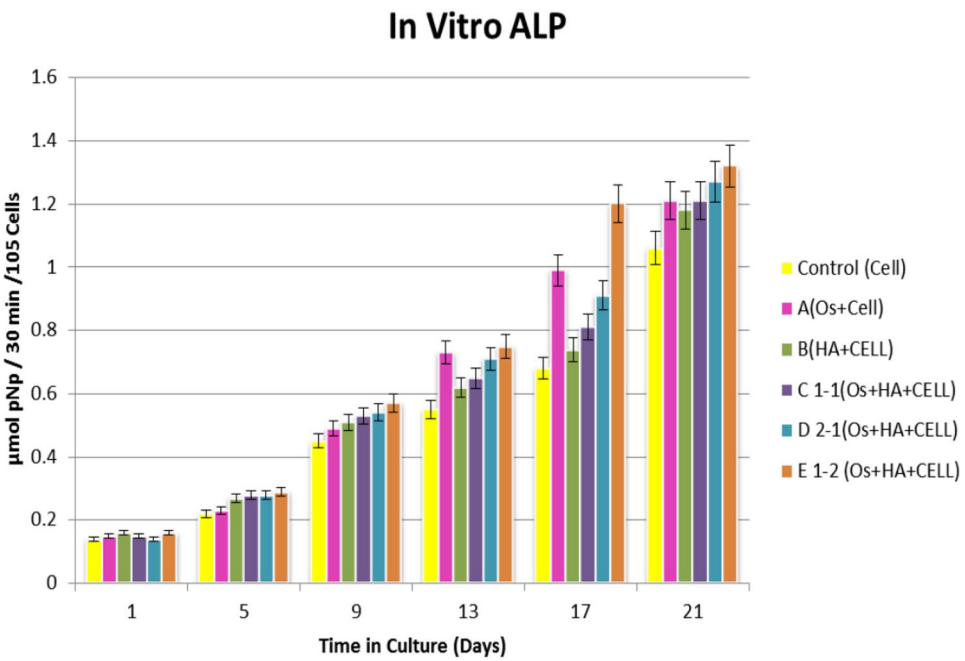

Fig. 11 ALP activity in different test groups on days 1, 5, 9, 13, 17, and 21 after osteoinduction. Group E showed the maximum expression in each time point

1:2 exhibited the highest ALP activity, suggesting its potential to promote osteogenic differentiation and mimic the effects of bone morphogenic protein-2, ultimately contributing to the development of bone tissue (Fig. 11).

4 Discussion

In this study, a novel bone tissue engineering scaffold was developed by combining ostrich eggshell (OE) and HA (Hydroxyapatite) at different ratios, resulting in various types of OE/HA scaffolds. The scaffolds were characterized using different techniques. FTIR (Fourier Transform Infrared) analysis of three different powder scaffolds (labeled as A, B, and C) yielded three distinct FTIR spectra, confirming the presence of OE and HA as the source compounds. In spectrum A, the peaks observed at 875 cm^{-1} and 1420 cm^{-1} indicated the presence of calcite, while the peaks at 564 cm-1 and 1035 cm^{-1} were related to the PO_4^{-3} group of HA [36]. A minor bent was observed in group D, which suggests a higher proportion of OE material compared to HA, with a ratio of 2:1 in group A. In group B, the width of the IR spectra for the PO4-3 bent at 564 cm^{-1} and 1036 cm^{-1} resembled the HA curve, while other peaks associated with OE appeared very weak and had a low width at 876 cm^{-1} and 1423 cm^{-1}. This indicates a stronger presence of HA compared to OE. According to Table 2, HA is twice as abundant as OE in this composition based on their molecular weight. Group C exhibited a better width for both components of OE and HA. The peaks in this powdered scaffold were stronger for both PO4-3 (564 cm^{-1} and 1036 cm^{-1}) and calcite (875 cm^{-1} and 1422 cm^{-1}). This provides evidence for the usage of an equal measure of both components as a scaffold [22]. The FTIR spectra revealed specific peaks indicative of calcite and the PO4-3 group of HA. The analysis showed that in group A, the ratio of OE to HA was 2:1, as evidenced by a minor bent in the spectrum. Group B demonstrated a stronger presence of HA compared to OE, while group C exhibited a better balance between the two components. These findings suggest that by adjusting the ratios of OE and HA, the composition of the scaffolds can be controlled, potentially influencing their suitability for bone tissue engineering applications.

XRD (X-ray Diffraction) analysis revealed that CaCO3 from ostrich eggshell (OE) and $Ca_5(PO_4)_3$ OH of from hydroxyapatite (HA) are the main compounds present in the three different OE/HA scaffolds. The results confirmed that the calcite content in sample A (OE:HA ratio of 2:1) is higher than the calcium phosphate hydroxide content, as shown in Table 3 and Fig. 2. The calcite score was determined to be 89 in this sample, compared to a calcium phosphate hydroxide score of 44 [38]. In sample B, test peaks of calcium phosphate hydroxide were visible compared to calcium carbonate. This finding was supported by Table 3, which showed a score of 65 for calcium phosphate hydroxide in this powdered scaffold, while the peak of ostrich eggshell was very weak. In material group C, the XRD pattern indicated nearly equal scores for both calcium carbonate and calcium phosphate hydroxide, indicating the successful integration of both material sources [24]. Radiographic analysis of the materials indicated that OE powder

exhibited a radiopacity similar to HA powder. However, the mixture of both powdered materials showed improved radiopacity. In comparison, the mixture of OE/HA, HA, and OE powders exhibited lower radiopacity due to the granular structure of OE. This phenomenon can be attributed to the granule structure of ostrich eggshell (Fig. 3D). The correct design of integrating both material sources was confirmed [24]. In sample B, surface lacuna and porosity were higher compared to the other samples, primarily due to the presence of more HA (with a rod-like shape) and fewer OE (with a sheet-like shape) granules. The higher the content of HA, the larger the surface area of the OE/HA scaffold. The increased surface area provides a better environment for cell adhesion. Cell attachment to the scaffold surface can be facilitated by enlarging the cytoplasm and/or forming cellular pedicles (41).

Sample A, with a ratio of 2 parts OE to 1 part HA, exhibited a higher calcite content compared to calcium phosphate hydroxide. In sample B, the presence of calcium phosphate hydroxide was more prominent compared to calcium carbonate. Sample C demonstrated almost equal scores for both calcium carbonate and calcium phosphate hydroxide, indicating successful integration of both materials. Radiographic analysis revealed that the mixture of OE and HA powders had improved radiopacity compared to individual powders. However, the radiopacity of the mixture was lower than that of pure HA or OE powders due to the granular structure of OE. Sample B exhibited higher surface lacuna and porosity, attributed to the higher content of HA with a rod-like shape and fewer OE granules with a sheet-like shape. The increased surface area in the OE/HA scaffold provides a favorable environment for cell adhesion, as cells can attach to the scaffold surface by enlarging the cytoplasm or forming cellular pedicles.

Before being analyzed in functional studies, a synthesized scaffold must undergo cytotoxicity studies [35]. L929 fibroblast-like cells are commonly used for cytotoxicity testing [29]. Passage 3 L929 cells with number of 0.5×10^3 were cultured in each wells of 6 well plate for 24 h with different types of OE/HA scaffolds. No signs of cellular damage were observed during this incubation period [30]. Light micrographs did not show any signs of apoptosis or vacuolated cells. These observations indicate that the fabricated scaffolds are non-toxic and possess desirable cytocompatibility properties [31]. Materials containing hydroxyapatite are often combined with other substances to enhance cell proliferation on the biomaterial. The presence of these additional elements can influence the acceptance of the material by cells. In some cases, the available zone is measured, and a zone less than 0.33 mm is considered acceptable for further work. In our study, no zone was observed in the OE/HA materials across all test groups with different material ratios [32]. Isolated RADMSCs (Rabbit Adipose-Derived Mesenchymal Stem Cells) were cultured in flasks to expand their numbers for subsequent experiments. Passage 4 cells were cultured under both 2D and 3D conditions, and evaluations of cell growth showed higher cell proliferation in the 3D conditions (Fig. 6) [33]. After isolating RADMSCs from rabbit adipose tissue, surface expression of mesenchymal stem cell-specific markers was analyzed using flow cytometry. CD45 and CD34 were used as negative markers, while CD90 and CD105 were selected as positive markers for these cells (Fig. 7) [14].

RADMSCs' adhesion to the scaffold surface was investigated using SEM. The images revealed that the cells extended their cytoplasm and formed cellular pedicles towards the scaffold surface. At a magnification of 5,000x, visible areas of cell membrane attachment to the surfaces of OE/HA granules were observed. This suggests that the rough edges of OE granules possess osteoconductive properties, providing a suitable niche for RADMSCs' adhesion, proliferation, and osteogenic differentiation, resembling real conditions of bone regeneration In a study by Xie et al. in 2016, SEM images at high magnifications showed thick layers and dense appetite around a spherical shape in the composite with a flower-like shape. In comparison, our material exhibited a sheet layer with specific lacunae for cell attachment in the dosage of 1–2 of OE/HA material [32]. To confirm that the powder scaffold is not cytotoxic, the attached cells were stained with DAPI and Annexin V/PI. Fluorescent micrograph analyses showed blue dots in the DAPI staining, indicating viable cell nuclei (Fig. 9) [37]. Annexin-PI stain colored the cytoplasmic fibril in green and the live nucleus in red (Fig. 10). In a study by Tsai et al. in 2019, which investigated cellular responses to HA/PCL scaffold, cells exhibited proper adhesive properties as shown by DAPI staining. Similar to their study, our study demonstrated that HA in combination with OE provided suitable niches for RADMSCs' adhesion. The best cellular attachment was observed in the OE:HA ratio of 1:2, specifically sample 2.

The osteogenic activity of the cultured RADMSCs in the presence of scaffolds was assessed by measuring ALP activity. Over time, ALP expression/activity increased following cell culture on the scaffolds. In the initial days of ALP measurement, ALP showed a gradual increase, which was accompanied by an increase in cell proliferation. Among all the scaffolds, sample 2 (with an OE:HA ratio of 1:2) exhibited the highest ability to enhance ALP levels. Increased ALP activity indicates a higher osteoconductive capability of the scaffold. In a study by Eeva Castrén and colleagues in 2015, ALP activity of cultured bone marrow-derived mesenchymal stromal cells (BMSCs) was higher in 3D culture compared to 2D cultures. They showed that under 2D conditions, ALP activity increased until day 14, while under 3D conditions, ALP increase was sustained until day 21 [38]. In our study, ALP activity increased significantly from day 9 onwards until day 21 in the presence of an OE/HA scaffold.

5 Conclusion

In conclusion based on the information provided in the passage. The study demonstrated that the combination of hydroxyapatite (HA) and ostrich eggshell (OE) resulted in the development of a non-cytotoxic scaffold that supported the adhesion, proliferation, and osteogenic differentiation of RADMSCs (Rabbit Adipose-Derived Mesenchymal Stem Cells). These findings suggest that the scaffold has the potential to be used in bone tissue engineering applications, such as bone defect reconstruction and fracture healing. However, further investigations are needed to fully validate the scaffold's safety and functionality. Additional in vitro and in vivo studies would be required to confirm its efficacy in bone engineering and to understand the underlying molecular mechanisms responsible for its osteogenic activity. These future studies would provide more comprehensive insights into the scaffold's potential and pave the way for its practical application in regenerative medicine.

Acknowledgements This article is based on the dissertation from the PhD program at Amol Azad University, Iran, and Golestan University of Medical Sciences, Iran. The research was conducted in accordance with the ethical guidelines of Golestan University of Medical Sciences (ID No: IR.GOUMS.REC.1397.25). We would like to express our gratitude to all the colleagues who provided assistance during this research."

Author contributions FA carried out design of the study, performing experiment, writing draft of manuscript and analyzing of SEM results. EF Participated in analysis of characterization of materials. MS participated in the interpretation of results. MM participated in the design of the study and performed the statistical analysis, interpretation of results and writing discussion. All authors read and approved the final manuscript.

Funding The authors have not disclosed any funding.

Data availability This study is original, and our hypothesis was proposed for the first time. Our research investigates the effects of natural biomaterials on stem cells, offering novel insights into this field. The findings presented in this study are supported by data from relevant references, as indicated in the reference section of this article. All authors affirm the authenticity of the data generated through diligent research and experimentation.

Declarations

Competing interests The authors declare no competing interests.

References

1. Gayathri V, Harikrishnan V, Mohanan PV. Vol. 2016, International Journal of Biomaterials. Hindawi; 2016 [cited 2020 Aug 18]. p. e1067857 Integration of rabbit adipose derived mesenchymal stem cells to hydroxyapatite burr hole button device for bone interface regeneration. Available from: https://www.hindawi.com/journals/ijbm/2016/1067857/.
2. Garrison KR, Donell S, Ryder J, Shemilt I, Mugford M, Harvey I, et al. Clinical effectiveness and cost-effectiveness of bone morphogenetic proteins in the non-healing of fractures and spinal fusion: a systematic review. Health Technol Assess Winch Engl. 2007;11(30):1–150.
3. Goudriaan WA, Harsevoort GJ, van Leeuwen M, Franken AA, Janus GJM. Incidence and treatment of femur fractures in adults with osteogenesis imperfecta: an analysis of an expert clinic of 216 patients. Eur J Trauma Emerg Surg. 2018. https://doi.org/10.1007/s00068-018-1005-9.
4. Wang W, Yeung KWK. Bone grafts and biomaterials substitutes for bone defect repair: a review. Bioact Mater. 2017;2(4):224–47.
5. Fernandez Grado G, Keller L, Idoux-Gillet Y, Wagner Q, Musset AM, Benkirane-Jessel N, et al. Bone substitutes: a review of their characteristics, clinical use, and perspectives for large bone defects management. J Tissue Eng. 2018;9:2041731418776819.
6. Pierannunzii L, Zagra L. Bone grafts, bone graft extenders, substitutes and enhancers for acetabular reconstruction in revision total hip arthroplasty. EFORT Open Rev. 2016;1(12):431–9.
7. Radha G, Manjubaashini N, Balakumar S. Nano-hydroxyapatite/natural polymer composite scaffolds for bone tissue engineering: a brief review of recent trend. Vitro Models. 2023. https://doi.org/10.1007/s44164-023-00049-w.
8. Jahanshahi M, Mofidian R, Hosseini SS, Miansari M. Investigation of mechanical properties of granular γ-alumina using experimental nano indentation and nano scratch tests. SN Appl Sci. 2023;5(6):164.
9. Soleymani S, Naghib SM. 3D and 4D printing hydroxyapatite-based scaffolds for bone tissue engineering and regeneration. Heliyon. 2023;9(9):e19363.

10. Rahman MS, Rana MM, Spitzhorn LS, Akhtar N, Hasan MZ, Choudhury N, et al. Fabrication of biocompatible porous scaffolds based on hydroxyapatite/collagen/chitosan composite for restoration of defected maxillofacial mandible bone. Prog Biomater. 2019;8(3):137–54.
11. Yadao RA, Lim G, Pe L, Valdez A, Cristobal S, Sunico ATC, et al. Ostrich eggshell as an onlay bone-graft substitute for orbital blow-out fractures. Philippine J Ophthalmol. 2004;29(3):127.
12. Li X, Lu X, Sun D, Wang X, Yang L, Zhao S, et al. Adipose-derived mesenchymal stem cells reduce lymphocytic infiltration in a rabbit model of induced autoimmune dacryoadenitis. Invest Ophthalmol Vis Sci. 2018;57(13):5161–70.
13. Khalilifar MA, Eslaminejad MB, Ghasemzadeh M, Hosseini S, Baharvand H. In vitro and in vivo comparison of different types of rabbit mesenchymal stem cells for cartilage repair. Cell J Yakhteh. 2019;21(2):150–60.
14. Pinto Filho STL, Pillat MM, Rosa MP, Dalmolin F, Ulrich H, Pippi NL, et al. Expression patterns of mesenchymal stem cell-specific proteins in adipose tissue-derived cells: possible immunosuppressing agent in partial allograft for restoring the urinary bladder in rabbits. Pesqui Veterinária Bras. 2018;38(12):2183–9.
15. Sharma A, Mawrie D, Magdalene D, Jaganathan BG. Isolation of multipotent mesenchymal stem cells from human extraocular muscle tissue. Bio-Protoc. 2019;9(4):e3167–e3167.
16. Zomer HD, Roballo KC, Lessa TB, Bressan FF, Gonçalves NN, Meirelles FV, et al. Distinct features of rabbit and human adipose-derived mesenchymal stem cells: implications for biotechnology and translational research. Stem Cells Cloning Adv Appl. 2018;23(11):43–54.
17. Naga SM, El-Maghraby HF, Sayed M, Saad EA. Highly porous scaffolds made of nanosized hydroxyapatite powder synthesized from egg-shells. J Ceram Sci Technol. 2015;6(3):237–44.
18. Caliman LB, da Silva SN, Junkes JA, Sagrillo VPD, Caliman LB, da Silva SN, et al. Ostrich eggshell as an alternative source of calcium ions for biomaterials synthesis. Mater Res. 2017;20(2):413–7.
19. Kontoyannis CG, Vagenas NV. Calcium carbonate phase analysis using XRD and FT-raman spectroscopy. Analyst. 2000;125(2):251–5.
20. Azami M, Jalilifiroozinezhad S, Mozafari M, Rabiee M. Synthesis and solubility of calcium fluoride/hydroxy-fluorapatite nanocrystals for dental applications. Ceram Int. 2011;37(6):2007–14.
21. Tsai WT, Hsien KJ, Hsu HC, Lin CM, Lin KY, Chiu CH. Utilization of ground eggshell waste as an adsorbent for the removal of dyes from aqueous solution. Bioresour Technol. 2008;99(6):1623–9.
22. Komath M, Varma HK. Development of a fully injectable calcium phosphate cement for orthopedic and dental applications. Bull Mater Sci. 2003;26(4):415–22.
23. Jrm F, Lhl L, Am C, Rlsb M, D N da R, Rm B, et al. Zinc-doped Calcium Phosphate Coating on Titanium Surface Using Ostrich Eggshell as a Ca2+ Ions Source. Biomater Med Appl [Internet]. 2018 May 22 [cited 2019 Nov 10];2017. Available from: https://www.scitechnol.com/abstract/zincdoped-calcium-phosphate-coating-on-titanium-surface-using-ostrich-eggshell-as-a-ca2-ions-source-6747.html.
24. Tan YH, Abdullah MO, Nolasco-Hipolito C, Taufiq-Yap YH. Waste ostrich- and chicken-eggshells as heterogeneous base catalyst for biodiesel production from used cooking oil: catalyst characterization and biodiesel yield performance. Appl Energy. 2015;15(160):58–70.
25. Geblinger D, Zink C, Spencer ND, Addadi L, Geiger B. Effects of surface microtopography on the assembly of the osteoclast resorption apparatus. J R Soc Interface. 2012;9(72):1599–608.
26. Romereim SM, Conoan NH, Chen B, Dudley AT. A dynamic cell adhesion surface regulates tissue architecture in growth plate cartilage. Dev Camb Engl. 2014;141(10):2085–95.
27. Hanks L, Casazza K, Ashraf A, Fernandez J. Calcium homeostasis may influence resting energy expenditure with effects most apparent in early pubertal girls. Acta Paediatr Oslo Nor. 2012;101(8):e363–8.
28. Mallineni SK, Nuvvula S, Matinlinna JP, Yiu CK, King NM. Biocompatibility of various dental materials in contemporary dentistry: a narrative insight. J Investig Clin Dent. 2013;4(1):9–19.
29. Anderson JM. Future challenges in the in vitro and in vivo evaluation of biomaterial biocompatibility. Regen Biomater. 2016;3(2):73–7.
30. Szymonowicz M, Korczynski M, Dobrzynski M, Zawisza K, Mikulewicz M, Karuga-Kuzniewska E, Zywicka B, Rybak Z, Wiglusz RJ. Cytotoxicity evaluation of high-temperature annealed nanohydroxyapatite in contact with fibroblast cells. Materials. 2017;10(6):590.
31. Sjerobabin N, Čolović B, Petrović M, Marković D, Živković S, Jokanović V. Cytotoxicity investigation of a new hydroxyapatite scaffold with improved structural design. Srp Arh Celok Lek. 2016;144(5–6):280–7.
32. Xie L, Yu H, Yang W, Zhu Z, Yue L. Preparation, in vitro degradability, cytotoxicity, and in vivo biocompatibility of porous hydroxyapatite whisker-reinforced poly(L-lactide) biocomposite scaffolds. J Biomater Sci Polym Ed. 2016;27(6):505–28.
33. Carter K, Lee HJ, Na KS, Fernandes-Cunha GM, Blanco IJ, Djalilian A, et al. Characterizing the impact of 2D and 3D culture conditions on the therapeutic effects of human mesenchymal stem cell secretome on corneal wound healing in vitro and ex vivo. Acta Biomater. 2019;99:247–57.
34. Won S, Huh YH, Cho LR, Lee HS, Byon ES, Park CJ. Cellular response of human bone marrow derived mesenchymal stem cells to titanium surfaces implanted with calcium and magnesium ions. Tissue Eng Regen Med. 2017;14(2):123–31.
35. Richards PD, Richards PA, Lee ME. Ultrastructural characteristics of ostrich eggshell: outer shell membrane and the calcified layers. J S Afr Vet Assoc. 2000;71(2):97–102.
36. Pasquinelli G, Tazzari P, Ricci F, Vaselli C, Buzzi M, Conte R, et al. Ultrastructural characteristics of human mesenchymal stromal (stem) cells derived from bone marrow and term placenta. Ultrastruct Pathol. 2007;31(1):23–31.
37. Liu C, Zhu C, Li J, Zhou P, Chen M, Yang H, et al. The effect of the fibre orientation of electrospun scaffolds on the matrix production of rabbit annulus fibrosus-derived stem cells. Bone Res. 2015;9(3):15012.
38. Castrén E, Sillat T, Oja S, Noro A, Laitinen A, Konttinen YT, Lehenkari P, Hukkanen M, Korhonen M. Osteogenic differentiation of mesenchymal stromal cells in two-dimensional and three-dimensional cultures without animal serum. Stem Cell Res Ther. 2015;6(1):1–3.